arXiv:2008.03335v1 [astro-ph.HE] 7 Aug 2020

MeV Gamma Rays from Fission:
A Distinct Signature of Actinide Production in Neutron Star Mergers

XILU WANG[1,2,*]
(N3AS COLLABORATION)
NICOLE VASSH[2]
(FIRE COLLABORATION)
TREVOR SPROUSE,[2,3,†] MATTHEW MUMPOWER,[3,4] RAMONA VOGT,[5] JORGEN RANDRUP,[6] AND REBECCA SURMAN[2]

[1]*Department of Physics, University of California, Berkeley, CA 94720, USA*
[2]*Department of Physics, University of Notre Dame, Notre Dame, IN 46556, USA*
[3]*Theoretical Division, Los Alamos National Laboratory, Los Alamos, NM, 87545, USA*
[4]*Center for Theoretical Astrophysics, Los Alamos National Laboratory, Los Alamos, NM, 87545, USA*
[5]*Lawrence Livermore National Laboratory, 7000 East Avenue, Livermore, CA 94550, USA*
[6]*Lawrence Berkeley National Laboratory, Nuclear Science Division, 1 Cyclotron Road, Berkeley, CA 94720, USA*

ABSTRACT

Neutron star mergers (NSMs) are the first verified site of rapid neutron capture (r-process) nucleosynthesis, and could emit gamma rays from the radioactive isotopes synthesized in the neutron-rich ejecta. These MeV gamma rays may provide a unique and direct probe of the NSM environment as well insight into the nature of the r process, just as observed gammas from the ^{56}Ni radioactive decay chain provide a window into supernova nucleosynthesis. In this work, we include the photons from fission processes for the first time in estimates of the MeV gamma-ray signal expected from a NSM event. We consider NSM ejecta compositions with a range of neutron richness and find a dramatic difference in the predicted signal depending on whether or not fissioning nuclei are produced. The difference is most striking at photon energies above ~ 3.5 MeV and at a relatively late time, several days after the merger event, when the ejecta is optically thin. We estimate that a Galactic NSM could be detectable by a next generation gamma-ray detector such as AMEGO in the MeV range, up to $\sim 10^4$ days after the merger, if fissioning nuclei are robustly produced in the event.

Keywords: Gamma-rays; Gamma-ray transient sources; Compact binary stars; Supernovae; Nucleosynthesis; R-process

1. INTRODUCTION

MeV gamma-rays ($E_\gamma \leq 10$ MeV) are emitted from newly synthesized radioactive nuclei and thus can provide a unique and direct probe of the nucleosynthesis and ejecta structure in astrophysical transients. One well-studied example of a transient nucleosynthetic event is a supernova (e.g., Clayton & Silk 1969; Bussard et al. 1989; The & Burrows 2014, and references therein). Supernovae, chiefly Type Ia, are dominant sources of iron-group elements (e.g., Nomoto et al. 1984, 2013, and references therein), and thus the gamma rays mainly come from the radioactive decay chain of ^{56}Ni

to ^{56}Co to ^{56}Fe. Gamma-ray observations of supernovae can precisely and directly measure ^{56}Ni yields, and the light curves encode a map of the structure and mixing of the ejecta (e.g., Bussard et al. 1989; The & Burrows 2014; Wang et al. 2019). Two nearby supernovae have been detected in MeV gamma rays so far, core-collapse supernova SN1987A (Matz et al. 1988; Teegarden et al. 1989) and Type-Ia supernova SN2014J (Churazov et al. 2014; Diehl et al. 2014).

Similar to supernovae, gamma rays also expected to be emitted from the isotopes synthesized in a neutron star merger (NSM) event. Unlike supernovae that produce mainly ^{56}Ni, NSMs are expected to produce a broad range of heavy radioactive isotopes via rapid neutron capture (r-process) nucleosynthesis. NSMs are the first verified r-process sites (Abbott et al. 2017), after the multi-messenger detection of GW170817, GRB170817A and the electromagnetic counterpart SSS17a/AT2017gfo (Abbott et al. 2017; Coulter et al.

Corresponding author: Xilu Wang, Nicole Vassh
xwang50@nd.edu, xlwang811@gmail.com,
nvassh@nd.edu, nvassh@gmail.com

* N3AS Postdoctoral Fellow
† Los Alamos CSES student fellow

2017; Goldstein et al. 2017; Savchenko et al. 2017; Valenti et al. 2017). The optical and infrared observations of this event indicated lanthanide production (Cowperthwaite et al. 2017; Kasen et al. 2017), however other than a tentative identification of strontium (Watson et al. 2019) no specific elemental yields could be determined (e.g., Pian et al. 2017; Shappee et al. 2017). Thus, while studies combining kilonova observations with other data from stars and simulations (e.g., Thielemann et al. 2017) make a strong case for NSMs to be a major or primary site of all r-process elements, there is still no direct evidence linking production of the heaviest elements such as gold, platinum, and the actinides with NSM outflows. Future observations may provide such evidence; Zhu et al. (2018) pointed out that if ^{254}Cf is produced in the event, its spontaneous fission and subsequent fission product decays can dominate late-time nuclear reheating, leading to a longer and brighter near-infrared kilonova signal. MeV gamma rays can provide complementary evidence, should the event occur nearby. Previous studies (Hotokezaka et al. 2016; Li 2019; Korobkin et al. 2020; Ruiz-Lapuente & Korobkin 2020) considered the MeV photons emitted from the β decay of radioactive r-process species and found such signals can encode key information on composition and event morphology.

An additional source of NSM MeV photons we consider here for the first time is the fission of actinide species. Fission reactions produce highly excited fragments that copiously emit neutrons and gammas over a large range of energies. If fissioning nuclei are present in the ejecta, the fission photons produced will contribute to the overall electromagnetic signal from the merger. This contribution is likely subdominant at early times, given the small number of fissioning species compared to those which β decay. However, at later times ($\gtrsim 10$ days), when the ejecta becomes optically thin[1], and most high Q-value β decays are complete, fission may become the dominant source for gamma-ray photons of multiple-MeV energies. Such a signal thus holds the potential to provide unambiguous evidence of actinide production in the merger event.

In this letter we provide a first estimate of the late-time, high energy MeV signal from a Galactic NSM event. We start from calculations of element synthesis and prompt spectra of photons emitted from fission and β decay. We process the emitted spectra through a semi-analytical radiation transfer model to estimate the time at which the MeV photons free-stream and simulate potential light curves and spectra. Finally we evaluate the detectability of a fission gamma signal in the next generation MeV telescope AMEGO (McEnery et al. 2019)[2] and find that a Galactic event would be detectable in the MeV range up to $\sim 10^4$ days after the merger.

2. PROMPT GAMMA-RAY SPECTRA OF r-PROCESS NUCLEI

The energy release from fission is larger than other processes occurring in the r process given its $\sim$200 MeV Q-value. Although most of the energy released is allocated to the total kinetic energy (TKE) of the newly formed fission fragments (~ 170 MeV), these fragments are also created with a substantial excitation energy such that their de-excitation can easily lead to the prompt emission of neutrons and gammas in the MeV range. Fission gamma spectra exhibit a wide range of MeV gamma emission as the fragments de-excite toward their more stable ground-state configurations. High energy statistical gammas are emitted through E1 (electric dipole radiation) and the giant dipole resonance while emission at energies less than $\sim$2-3 MeV are dominated by E2 (electric quadrupole radiation) transitions between nuclear levels.

An example fission gamma spectrum is shown in Figure 1 for ^{252}Cf, a species which primarily decays through α-decay but has a 3% spontaneous fission branching ratio and a half-life of 2.6 years. The prompt fission gamma spectrum of ^{252}Cf is well-studied; two experimental data sets (Billnert et al. 2013; Qi et al. 2018) are included in Figure 1. As this example illustrates, fission can result in gamma emission with energies as high as $\sim$8 MeV.

Other decay processes which take place on the timescales of interest for detection of electromagnetic signals from NSMs are β and α decay. In an α decay, most of the energy is released as the kinetic energy of the α particle and the decay radiation is dominated by sub-MeV x-rays. Thus here we consider how the gamma emission from fission is distinguishable from that of β decay. We calculate the β-decay gamma-ray spectrum for each nucleus i as

$$\frac{dN_{\gamma,i}^{\beta^-}}{dE} = RP_{i,\beta^-}(E) + \sum_{E'} \mathcal{I}_{i,\beta^-}(E')\delta(E - E'), \quad (1)$$

using a combination of individual lines at discrete energies E and absolute intensity $\mathcal{I}(E)$ with a Dirac δ function distribution, as well as a possible continuum component $RP(E)$. In order to evaluate Eq. 1, we require the spectra associated with individual decays encoded in the functions $\mathcal{I}$ and RP. For these β-decay spectra, we adopt data from ENDF/B-VIII.0[3] (Brown et al. 2018) and, when unavailable, we supplement

---

[1] The observations of SSS17a/AT2017gfo and theoretical studies (e.g., Pian et al. 2017; Drout et al. 2017; Kilpatrick et al. 2017; Shappee et al. 2017; Waxman et al. 2019) suggest that the timescale when the ejecta becomes optically thin is about a few days after the merger moment.

[2] https://asd.gsfc.nasa.gov/amego/index.html

[3] https://www-nds.iaea.org/public/download-endf/ENDF-B-VIII.0/

with spectra calculated in the Los Alamos QRPA+HF framework (Mumpower et al. 2016; Möller et al. 2019).

The distinct nature of the gamma emission from fission as compared to β-decay is evident from considering the β-decay gamma spectrum of a nucleus populated on timescales of days in the r process, ^{125}Sn. Exotic r-process nuclei with high Q_β values typically decay on very fast ($\sim$seconds or less) timescales. As can be seen from Figure 1, β-decay gamma spectra of interest at later times typically fall off after $\sim$3 MeV. This presents an opportunity for gamma-ray telescopes to confirm the synthesis of heavy, fissioning actinides in a merger event through the detection of gammas in the $\sim$3-10 MeV energy range unique to the fission process.

To obtain the individual fission gamma spectra for all the neutron-rich actinides which could be accessed by a merger event and for which experimental data is not available, we use the 2016 version of the code GEF (Schmidt et al. 2016) as in Vassh et al. (2019). Since the energetics of prompt emission from excited fragments which determines the fission gamma spectra is an active area of study, we investigate model dependence using the FREYA code (Vogt & Randrup 2017; Verbeke et al. 2018). We implement FREYA as described in Vassh et al. (2019) with the TKE and fission yields predicted by GEF taken as inputs for FREYA. The theoretical fission gamma spectra for ^{252}Cf calculated with GEF and FREYA are compared to the experimental data in Figure 1.

FREYA and GEF take different approaches to modeling the de-excitation treatment of the fission fragments. FREYA emits neutrons until energetically forbidden, given the one neutron separation energy, and then emits gamma-ray photons to dissipate the remaining excitation energy. GEF, instead, uses phenomenological decay widths of neutron and photon emission, allowing competition between the two. Additionally, the two codes differ in their treatments of level transitions which affect the low energy fission gamma spectrum below $\sim$2 MeV. This region of larger differences between the treatments in the two codes, as seen in Fig. 1, will be dominated by gammas emitted by β-decays in the r process. From $\sim$3-8 MeV, where the GEF and FREYA results are similar, the spectrum is dominated by the giant dipole resonance. For energies above $\sim$8 MeV, the neutron-gamma competition in GEF leads to a pronounced high energy tail relative to FREYA. Importantly, despite all of the distinct approaches for modeling the de-excitation of fission fragments, the GEF and FREYA results for fission spectra are compatible from $\sim$3-8 MeV in showing a pronounced higher energy distribution. The consistency of the theoretical calculations and experimental data support our exploration of fission gamma emission at energies above 3 MeV as a potential r-process observable.

3. RADIATION TRANSFER CALCULATION
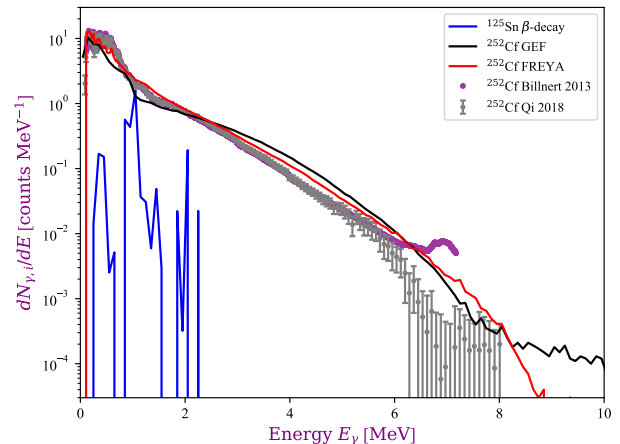
Figure 1. The calculated prompt gamma spectra emitted from the spontaneous fission of ^{252}Cf using GEF (black line) and FREYA (red line), as compared with experimental data from Billnert et al. (2013) (purple dots) and Qi et al. (2018) (grey dots). The prompt gamma spectra emitted from the β-decay of the ^{125}Sn ground state (blue line) taken from ENDF/B-VIII.0 is also shown.

Since our aim is to investigate the role of fission in the gamma-ray emissions from a NSM, we focus on late times after $\sim$ 10 days when the gamma-ray signals due to fission could emerge. Thus, a semi-analytical calculation is adequate to compute the gamma-ray emissions observed after the propagation inside the NSM ejecta at this late time when the ejecta is nearly optically thin.

To estimate the light curve and spectrum observed on Earth, we adapt the radiation transfer calculations from Wang et al. (2019) with a uniform ejecta model for the r-process ejecta. First, we assume the ejecta consists of a dense core plus a less dense shell and is expanding homologously, i.e., $v(r) \propto r$. Here, the radius from the center is $r \sim vt$, and the maximum velocity at the outermost radius is v_0. The total ejecta mass is $M_{\rm ej}$, with a fraction f of the mass distributed at the shell of the ejecta with radius $a(t)$ and density $\rho_2(t)$, while the remaining is in the core with radius $R(t)$, density $\rho_1(t)$, and subtended angle $\theta_1 \sim R/D$, where D is the distance between the Earth and the NSM. The angle subtended by the shell is between θ_1 and $\theta_2 \sim a/D$. Thus the ejecta emission is in the region between $\pm\theta_2$. A sketch of this ejecta model appears in Fig. 2. These ejecta parameters will serve as inputs to the radiation transfer calculations, yielding estimates of the observable γ-ray light curves and spectra.

Combining the prompt emitted photon spectra $dN_{\gamma,i}(E)/dE$ from each nucleus i through fission and β decay, with their relative nuclear abundances $Y_i(t)$ as function of time t and decay rates obtained from our r-process nucleosynthesis calculations, the emitted gamma-ray luminosity is then cal-
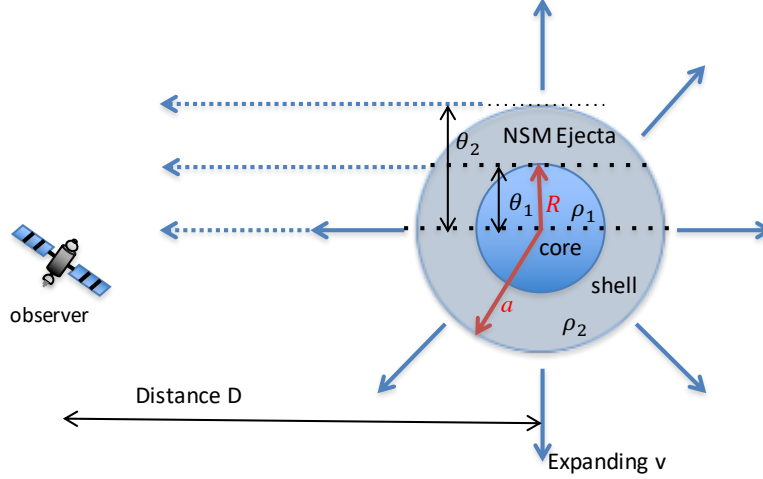
Figure 2. Sketch of the r-process ejecta model from a NSM. The distance between the observer and the NSM is D. In this model, the ejecta radius is a, subtended angle θ_2. The r-process material is distributed in the shell of the ejecta with mass percentage f and density ρ_2, and in the core with remaining mass, with radius R, subtended angle θ_1, and density ρ_2.

culated as

$$
\begin{aligned}
L_{\gamma,\mathrm{em}}(E) &= \frac{dN_{\gamma,\mathrm{em}}(E)}{dEdt} \\
&= \frac{M_{\mathrm{ej}}}{m_{\mathrm{p}}}\bigg(\sum_i \lambda_{i,\beta^-} Y_i(t) \times \frac{dN_{\gamma,i}^{\beta^-}(E)}{dE} \\
&\quad + \sum_j \lambda_{j,\mathrm{fission}} Y_j(t) \times \frac{dN_{\gamma,j}^{\mathrm{fission}}(E)}{dE}\bigg),
\end{aligned} \quad (2)
$$

where m_{p} is the proton mass, λ_{β^-} is the partial decay rate which is derived from the half-life and β-decay branching ratio, and $\lambda_{\mathrm{fission}}$ is the fission rate. The nucleosynthetic yields are obtained using the nuclear reaction network code Portable Routines for Integrated nucleoSynthesis Modeling, or PRISM (Mumpower et al. 2018). Experimental half lives and rates are used whenever possible; otherwise we adopt the theoretical nuclear data applied in Vassh et al. (2019); Wang et al. (2020) which makes use of GEF fission yields along with FRDM2012 masses and FRLDM fission barriers.

To propagate the emitted gamma rays through the ejecta, we solve the radiative transfer equation $dI_E/dl = -\alpha(E)I_E + j_E$, with the absorption coefficient $\alpha(E) = \rho\kappa(E)$, where $\kappa(E)$ is the opacity of the dense ejecta material through which the photons propagate. Here, the source term is $j_E = L_{\gamma,\mathrm{em}}(E)/4\pi V$. The opacity values of the r-process isotopes are adopted from XCOM website[4], for photon interactions including coherent (Rayleigh) scattering, incoherent (Compton) scattering, photoelectric absorption, and pair production. Only non-scattered photons are included in the observed gamma-ray signal here; scattered photons are ignored

as their effects are minimal at late times when the ejecta is nearly optically thin.

We calculate the opacities in the MeV energy range of the r-process ejecta based on its composition with a mixture of the opacities of five characteristic isotopes (Fe, Xe, Eu, Pt and U). That is, we adopt the opacity of iron for elements with mass number $A \leq 109$, xenon for $110 \leq A \leq 137$, europium for $138 \leq A \leq 178$, platinum for $179 \leq A \leq 219$, and uranium for $A \geq 220$.

The intensity I along a line of sight with angle θ, in the region with density ρ and path length between l_0 and l_m (the maximum path length for the photons in the line of sight is $l_{\max} = 2\sqrt{a^2 - (D\theta)^2}$), observed at energy E_i after the Doppler shift is thus:

$$
\begin{aligned}
I_{E_i}(\theta, l_m) &= \frac{dN_{\gamma,\mathrm{ob}}}{dEdtdAd\Omega} \\
&= I_{E_i}(0)e^{-(\tau(E_i,l_{\max})-\tau(E_i,0))} \\
&\quad + \int_{l_0}^{l_m} j_{E_0'(\tau'(E_0',l))}e^{-(\tau(E_0,l_m)-\tau'(E_0',l))}dl,
\end{aligned} \quad (3)
$$

where the optical depth $\tau(E) = \int \rho_{\mathrm{ej}}\kappa(E)dl = \tau_a(E)l/a$, l is the photon path length, and E_0 is the initial energy of a photon emitted with $E_0(\theta,l) = E_i/[1 + (v/c)(l/a - l_{\max}/2a)]$.

For the r-process ejecta sketched in Figure 2, if the line of sight travels through the same region ($\theta_1 \leq \theta \leq \theta_2$), the total intensity along the line of sight is $I_{E_i,1}(\theta) = I_{E_i}(\theta, l_{\max})$ with $l_0 = 0$. If the line of sight travels through different regions ($0 \leq \theta \leq \theta_1$), the total intensity $I_{E_i,2}(\theta)$ includes stacking the calculation of Eq. 3 for each region, from the path length $l = 0$ until $l_{\max}$.

Finally, the total flux from the r-process shell plus core ejecta is an integral of the intensity over the solid angle sub-

tended by the ejecta, i.e.,

$$F_{E_i}(t) = \frac{dN_{\gamma,\text{ob}}}{dEdtdA} = \int I_{E_i}(\theta)\cos\theta d\Omega$$

$$\approx 2\pi \left(\int_0^{\theta_1} I_{E_i,1}(\theta)\theta d\theta + \int_{\theta_1}^{\theta_2} I_{E_i,2}(\theta)\theta d\theta \right),$$

$$F(t) = \int F_{E_i}(t)dE_i. \qquad (4)$$

We select $M_{\text{ej}} = 0.01 M_\odot$ (e.g., Bovard et al. 2017), $v_0 = 0.3c$ (e.g., Shappee et al. 2017), i.e., $\beta = 0.3$, $\rho_{1,initial} = 2 \times 10^{10}\text{g/cm}^3$, $\rho_{2,initial} = 2 \times 10^7\text{g/cm}^3$ (Rosswog et al. 2013; Piran et al. 2013) with shell fraction $f = 10\%$. We use a fiducial distance $D = 10$ kpc for a Galactic NSM; for other choices of distance, the flux and count rates will scale as $(10\,\text{kpc}/D)^2$. Variations in these astrophysical parameters result in only modest changes to our simulation results in terms of signal magnitude and the time when the eject becomes optically thin, and do not influence the qualitative conclusions of Section 4.

4. PREDICTED MEV GAMMA-RAY SIGNALS FROM NSMS

4.1. *Very neutron-rich ejecta with robust fission*

In very neutron-rich ejecta, the r process pushes its reach into the heavy, neutron-rich actinides until the synthesis is ultimately terminated by fission. Here we adopt conditions from the very neutron-rich ($Y_e \sim 0.015$) dynamical ejecta tidal-tail simulations of Rosswog et al. (2013); Piran et al. (2013). Figure 3 shows the resulting spectra at 10 days and 1000 days after merger, calculated as described in Section 3. Comparing the contributions to the spectra from β-decay and fission, we find that above ~3.5 MeV late-time gamma emission is dominated by high energy fission gammas, as expected from Section 2. In addition, we find that the gamma-ray spectra from fission and β-decays are parallel between ~3.5 to 8 MeV, indicating that the β-decay photons in this energy range mainly originate from the high Q_β-value decays of the exotic, short-lived fission fragments.

To better evaluate the evolution of the MeV gamma-ray signals from fission and β-decays, we simulate the light curves above ~ 3.5 MeV, as shown in Figure 4. Comparing the light curves before and after radiation transfer shows that for this neutron-rich outflow—and given our ejecta model and the parameter choices described in section 3—the ejecta becomes optically thin after ~ 10 days. We find that, for photons in this higher MeV energy range, the gamma-ray signal from fission begins to dominate over the β-decay gamma emission after ~1 day. The light curve plateaus correspond to the fissioning species decaying on long timescales which, given the theoretical nuclear data applied in this calculation, are ^{254}Cf between 1 day and several hundred days as well as
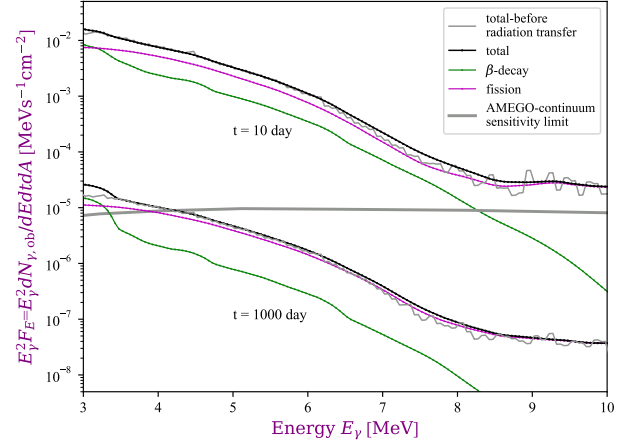
Figure 3. Gamma-ray spectra at 10 and 1000 days given very neutron-rich ejecta from an NSM located at 10 kpc. Gray lines show the total prompt gamma-ray signal emitted, while black lines show the total signal after our radiation transfer calculation. Green lines show the contribution from β-decays to the observable gamma-ray signal, while the purple lines show the contribution from fission. The grey shaded band shows the sensitivity limit range for the AMEGO detector.
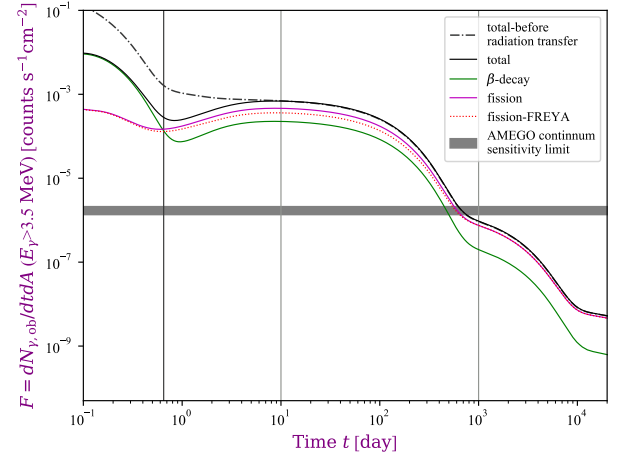
Figure 4. The predicted gamma-ray light curves at energies above 3.5 MeV given very neutron-rich ejecta from an NSM located at 10 kpc. Line color notations are the same as Figure 3. The result given the prompt photon spectrum of ^{254}Cf fission found when photon emission is calculated using FREYA instead of GEF (red dotted line) is also shown.

^{252}Cf between 1000 and 10000 days. Compared to the sensitivity limit of AMEGO, both the spectra and light curve suggest that a Galactic NSM would be observable by AMEGO at energies above 3.5 MeV before ~1000 days after the merger event.

We evaluate the sensitivity of our findings to the different predictions for prompt fission gamma spectra discussed in Section 2 by examining the light curve when the FREYA calculation for ^{254}Cf prompt gamma emission is implemented in our calculations. The gamma-ray light curve with the FREYA treatment from prompt emission has a similar shape and magnitude to that of GEF. Therefore although there remain many complexities in modeling the prompt emission from neutron-rich fission fragments, as long as the fissioning species have a non-negligible high energy (> 3.5 MeV) tail, as is supported by experiment, our conclusions regarding the the unique ability of fission to provide a signal in this energy range remain the same.

Additional nuclear physics uncertainties influence theoretical calculations of the β-decay and fission rates that determine which fissioning nuclei can be populated during the r process. We therefore repeat our analysis using fission rates obtained with alternate fission barrier models, as in Vassh et al. (2019). We find that although the abundance of fissioning species, as well as which fissioning nuclei play a role in late-time gamma emission, depend on the nuclear model, our main conclusions remain unchanged. Even the lowest predicted light curve—that obtained implementing Thomas-Fermi fission barriers, which lead to a ^{254}Cf abundance two orders of magnitude smaller than that of Fig. 4 (Vassh et al. 2019)—is above the sensitivity limit of AMEGO from ~10-100 days. We leave a more detailed investigation of the nuclear model dependence of the MeV fission gamma signature to be explored in follow-up work.

4.2. *Variations on neutron-richness and the participation of fission*

Since our results with very neutron-rich dynamical ejecta in the previous section show that outflow conditions which robustly reach fissioning species could produce a detectable MeV fission gamma-ray signal from a Galactic NSM, we next consider ejecta with a variety of neutron richness. We start with parameterized outflow conditions with low entropy ($s/k_B = 30$), long timescale ($\tau = 70$ ms), and a range of initial electron fractions $Y_e = 0.15 - 0.3$, which represents conditions that could be found in both NSM dynamical and wind ejecta (Radice et al. 2018; Just et al. 2015). This will produce a variation of nuclei that can be synthesized, as well as the overall abundance of actinide species, and therefore the degree to which fission participates in the r process. Since the ejecta composition determines the photon opacity as well as which nuclei emit MeV gammas, we expect that MeV gamma-ray signals will be sensitive to the nature of the outflow conditions present in NSMs.

Figure 5 shows the simulated gamma-ray light curves at photon energies above 3.5 MeV, as well as the spectra at 10 days after the merger, for outflows with $Y_e = 0.15$ (robust fis-
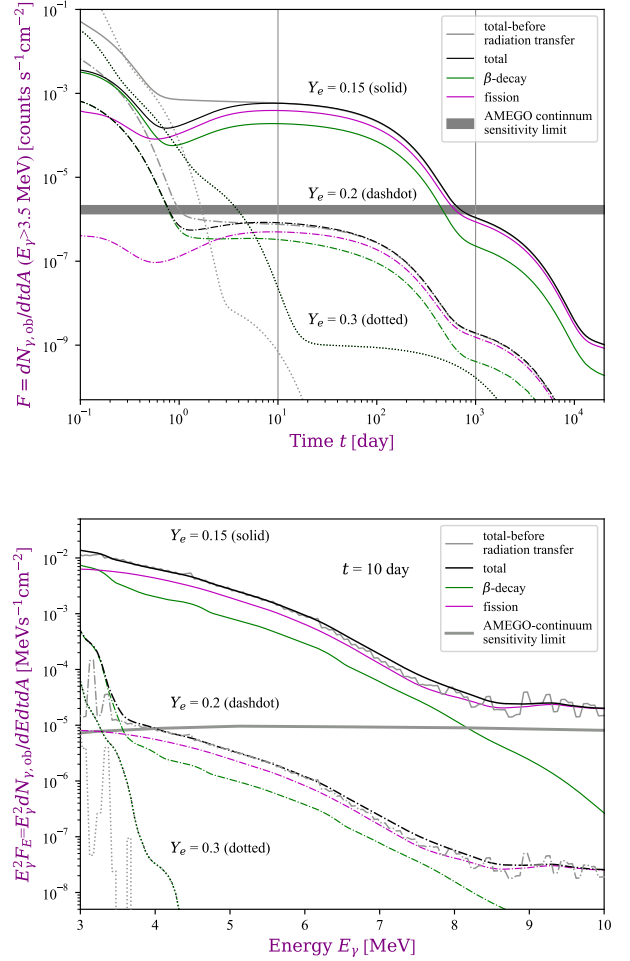
Figure 5. The predicted gamma-ray light curves at energies above 3.5 MeV (top) and the spectra at 10 days (bottom) given various levels of neutron-richness for a low entropy, long timescale outflow from an NSM located at 10 kpc. Line color notations are the same as Figure 3. An initial neutron-richness of $Y_e = 0.15$ (solid line) demonstrates the case which robustly reaches fissioning species, whereas the $Y_e = 0.2$ case (dash-dot line) shows a limited participation by fission and the $Y_e = 0.3$ case (dotted line) shows no participation by fission.

sion), $Y_e = 0.2$ (limited fission), and $Y_e = 0.3$ (no fission). We see that the light curve and spectra for this type of outflow with $Y_e = 0.15$ are similar to the results given the very neutron-rich ejecta considered in Figure 4, with the ejecta becoming optically thin after ~ 10 days and the gamma-ray signal at energies above 3.5 MeV being dominated by fission over β-decay after $\sim$1 day.

In contrast, the light curves and spectra given outflow conditions which are less neutron-rich and therefore see little to no synthesis of fissioning nuclei are dramatically different from results given very neutron-rich ejecta, with the case of limited fission seeing a drop of greater than three orders

of magnitude in the MeV gamma-ray signal above 3.5 MeV after $\sim$1 day. For gammas in this energy range, the signal is strongest when conditions support a robust participation of fissioning species, and is detectable before $\sim$1000 days, whereas, in the case of limited fission, the signal is just below the detectability threshold at $\sim$10-100 days. When fissioning nuclei are not populated, the signal is too faint to be detected.

We therefore find that the late-time gamma-ray signals from NSMs in the energy range > 3.5 MeV are very sensitive to the degree to which fission participates in r-process nucleosynthesis. If such a signal is detected from a Galactic NSM at times of several days or later, the outflow conditions must be such that they support the synthesis of fissioning actinide species. Such MeV gamma-ray observations of NSMs would therefore both provide direct evidence as to whether NSMs can explain the origins of the heaviest r-process species, and consequently lower mass number species such as gold, as well as probe the astrophysical properties of the ejecta such as neutron richness.

5. DISCUSSIONS AND CONCLUSIONS

In this paper, we report a first estimate for the contribution of fission to a late-time MeV gamma-ray signal from a Galactic NSM event. We find that gamma-ray emission above 3.5 MeV at timescales longer than $\sim$ 10 days is a direct consequence of fissioning nuclei synthesized during the event. This signal is therefore sensitive to the fission contribution, as determined by the nature of astrophysical outflows such as neutron richness. We find that if isotopes which fission on the order of days are significantly populated, the MeV gamma-ray signal predicted is above the sensitivity limit of the AMEGO detector. Thus, by exploring the energy range distinct to fission, next generation MeV gamma-ray detectors can shed light on the synthesis achievable by NSMs.

Given the rarity of neutron star binaries in our Galaxy and the sensitivities of MeV gamma-ray telescopes, the prospects for detecting MeV gamma-ray emission from fission in NSMs are challenging. However, the potential pay off of such an observation is dramatic since it could provide direct evidence for NSMs as a source of actinide elements. Thus our findings call for next generation MeV detectors like AMEGO or e-ASTROGAM or LOX (Fryer et al. 2019), which will provide a distinct and complementary approach to other observational methods aiming to understand the origin of r-process elements.

REFERENCES

Abbott, B. P., Abbott, R., Abbott, T. D., et al. 2017, ApJL, 848, L12, doi: 10.3847/2041-8213/aa91c9

Abbott et al., B. P. 2017, PhRvL, 119, 161101, doi: 10.1103/PhysRevLett.119.161101

Billnert, R., Hambsch, F. J., Oberstedt, A., & Oberstedt, S. 2013, PhRvC, 87, 024601, doi: 10.1103/PhysRevC.87.024601

Bovard, L., Martin, D., Guercilena, F., et al. 2017, PhRvD, 96, 124005, doi: 10.1103/PhysRevD.96.124005

Brown, D., Chadwick, M., Capote, R., et al. 2018, Nuclear Data Sheets, 148, 1 , doi: https://doi.org/10.1016/j.nds.2018.02.001

Bussard, R. W., Burrows, A., & The, L. S. 1989, ApJ, 341, 401, doi: 10.1086/167503

Churazov, E., Sunyaev, R., Isern, J., et al. 2014, Nature, 512, 406, doi: 10.1038/nature13672

Clayton, D. D., & Silk, J. 1969, ApJL, 158, L43, doi: 10.1086/180429

Coulter, D. A., Foley, R. J., Kilpatrick, C. D., et al. 2017, Science, 358, 1556, doi: 10.1126/science.aap9811

Cowperthwaite et al., P. S. 2017, ApJL, 848, L17

Diehl, R., Siegert, T., Hillebrandt, W., et al. 2014, Science, 345, 1162, doi: 10.1126/science.1254738

Drout, M. R., Piro, A. L., Shappee, B. J., et al. 2017, Science, 358, 1570, doi: 10.1126/science.aaq0049

Fryer, C. L., Timmes, F., Hungerford, A. L., et al. 2019, arXiv e-prints, arXiv:1902.02915. https://arxiv.org/abs/1902.02915

Goldstein, A., Veres, P., Burns, E., et al. 2017, ApJL, 848, L14, doi: 10.3847/2041-8213/aa8f41

Hotokezaka, K., Wanajo, S., Tanaka, M., et al. 2016, MNRAS, 459, 35, doi: 10.1093/mnras/stw404

Just, O., Bauswein, A., Pulpillo, R. A., Goriely, S., & Janka, H.-T. 2015, MNRAS, 448, 541, doi: 10.1093/mnras/stv009

Kasen, D., Metzger, B., Barnes, J., Quataert, E., & Ramirez-Ruiz, E. 2017, Nature, 551, 80, doi: 10.1038/nature24453

Kilpatrick, C. D., Foley, R. J., Kasen, D., et al. 2017, Science, 358, 1583, doi: 10.1126/science.aaq0073

Korobkin, O., Hungerford, A. M., Fryer, C. L., et al. 2020, ApJ, 889, 168, doi: 10.3847/1538-4357/ab64d8

Li, L.-X. 2019, ApJ, 872, 19, doi: 10.3847/1538-4357/aaf961

Matz, S. M., Share, G. H., Leising, M. D., Chupp, E. L., & Vestrand, W. T. 1988, Nature, 331, 416, doi: 10.1038/331416a0

McEnery, J., van der Horst, A., Dominguez, A., et al. 2019, in Bulletin of the American Astronomical Society, Vol. 51, 245

Möller, P., Mumpower, M. R., Kawano, T., & Myers, W. D. 2019, At. Data Nucl. Data Tables, 125, 1, doi: https://doi.org/10.1016/j.adt.2018.03.003

Mumpower, M. R., Kawano, T., & Möller, P. 2016, PhRvC, 94, 064317, doi: 10.1103/PhysRevC.94.064317

Mumpower, M. R., Kawano, T., Sprouse, T. M., et al. 2018, ApJ, 869, 14, doi: 10.3847/1538-4357/aaeaca

Nomoto, K., Kobayashi, C., & Tominaga, N. 2013, ARA&A, 51, 457, doi: 10.1146/annurev-astro-082812-140956

Nomoto, K., Thielemann, F. K., & Yokoi, K. 1984, ApJ, 286, 644, doi: 10.1086/162639

Pian, E., D'Avanzo, P., Benetti, S., et al. 2017, Nature, 551, 67, doi: 10.1038/nature24298

Piran, T., Nakar, E., & Rosswog, S. 2013, Mon. Not. R. Astron. Soc., 430, 2121, doi: 10.1093/mnras/stt037

Qi, L., Lebois, M., Wilson, J. N., et al. 2018, PhRvC, 98, 014612, doi: 10.1103/PhysRevC.98.014612

Radice, D., Perego, A., Hotokezaka, K., et al. 2018, ApJ, 869, 130, doi: 10.3847/1538-4357/aaf054

Rosswog, S., Piran, T., & Nakar, E. 2013, Mon. Not. R. Astron. Soc., 430, 2585, doi: 10.1093/mnras/sts708

Ruiz-Lapuente, P., & Korobkin, O. 2020, ApJ, 892, 45, doi: 10.3847/1538-4357/ab744e

Savchenko, V., Ferrigno, C., Kuulkers, E., et al. 2017, ApJL, 848, L15, doi: 10.3847/2041-8213/aa8f94

Schmidt, K.-H., Jurado, B., Amouroux, C., & Schmitt, C. 2016, Nucl. Data Sheets, 131, 107, doi: 10.1016/j.nds.2015.12.009

Shappee, B. J., Simon, J. D., Drout, M. R., et al. 2017, Science, 358, 1574, doi: 10.1126/science.aaq0186

Teegarden, B. J., Barthelmy, S. D., Gehrels, N., Tueller, J., & Leventhal, M. 1989, Nature, 339, 122, doi: 10.1038/339122a0

The, L.-S., & Burrows, A. 2014, ApJ, 786, 141, doi: 10.1088/0004-637X/786/2/141

Thielemann, F. K., Eichler, M., Panov, I. V., & Wehmeyer, B. 2017, Annual Review of Nuclear and Particle Science, 67, 253, doi: 10.1146/annurev-nucl-101916-123246

Valenti, S., Sand, D. J., Yang, S., et al. 2017, ApJL, 848, L24, doi: 10.3847/2041-8213/aa8edf

Vassh, N., Vogt, R., Surman, R., et al. 2019, Journal of Physics G Nuclear Physics, 46, 065202, doi: 10.1088/1361-6471/ab0bea

Verbeke, J. M., Randrup, J., & Vogt, R. 2018, Comp. Phys. Comm., 222, 263, doi: 10.1016/j.cpc.2017.09.006

Vogt, R., & Randrup, J. 2017, PhRvC, 96, 064620, doi: 10.1103/PhysRevC.96.064620

Wang, X., Fields, B. D., & Lien, A. Y. 2019, MNRAS, 486, 2910, doi: 10.1093/mnras/stz993

Wang, X., Fields, B. D., Mumpower, M., et al. 2020, ApJ, 893, 92, doi: 10.3847/1538-4357/ab7ffd

Watson, D., Hansen, C. J., Selsing, J., et al. 2019, Nature, 574, 497, doi: 10.1038/s41586-019-1676-3

Waxman, E., Ofek, E. O., & Kushnir, D. 2019, ApJ, 878, 93, doi: 10.3847/1538-4357/ab1f71

Zhu, Y., Wollaeger, R. T., Vassh, N., et al. 2018, ApJL, 863, L23, doi: 10.3847/2041-8213/aad5de